

^{56}Ni dredge-up in the type IIp Supernova 1995V

A.Fassia¹, W.P.S. Meikle¹, T.R. Geballe², N.A. Walton³, D.L. Pollacco³,
R.G.M. Rutten³, C. Tinney⁴

¹Astrophysics Group, Blackett Laboratory, Imperial College, Prince Consort Rd, London SW7 2BZ, UK

²Joint Astronomy Centre, 660 N. A'Ohoku Place, University Park, Hilo, Hawaii 96720, USA

³Royal Greenwich Observatory, Apartado de Correos 321, 38780 Santa Cruz de La Palma, Tenerife, Islas Canarias, Spain

⁴Anglo-Australian Observatory, PO Box 296 Epping, NSW 2121, Australia

Abstract

We present contemporary infrared and optical spectra of the plateau type II SN 1995V in NGC 1087 covering four epochs, approximately 22 to 84 days after shock breakout. The data show, for the first time, the *infrared* spectroscopic evolution during the plateau phase of a typical type II event. In the optical region P Cygni lines of the Balmer series and of metals such as Sc II, Fe II, Sr II, Ca II and Ba II lines were identified. The infrared (IR) spectra were largely dominated by the continuum, but P Cygni Paschen lines and Brackett γ lines were also clearly seen. The other prominent IR features are confined to wavelengths blueward of 11000 Å and include Sr II 10327, Fe II 10547, C I 10695 and He I 10830 Å. Helium has never before been unambiguously identified in a type IIp supernova spectrum during the plateau phase. We demonstrate the presence of He I 10830 Å on days 69 and 85. The presence of this line at such late times implies re-ionisation. A likely re-ionising mechanism is γ -ray deposition following the radioactive decay of ^{56}Ni . We examine this mechanism by constructing a spectral model for the He I 10830 Å line based on explosion model s15s7b2f of Weaver & Woosley (1993). We find that this does not generate the observed line owing to the confinement of the ^{56}Ni to the central zones of the ejecta. In order to reproduce the He I line, it was necessary to introduce additional upward mixing or “dredge-up” of the ^{56}Ni , with $\sim 10^{-5}$ of the total nickel mass reaching above the helium photosphere. In addition, we argue that the He I line-formation region is likely to have been in the form of pure helium clumps in the hydrogen envelope. The study of He I 10830 Å emission during the photospheric phase of core-collapse supernovae provides a promising tool for the constraint of initial mixing conditions in explosion models.

Key words: supernova, γ rays, mixing, infrared, spectra

1 Introduction

Type IIp (plateau) supernovae form the classic subgroup of the core-collapse supernovae. They are believed to arise from massive stars ($12\text{-}25 M_{\odot}$) during the red supergiant phase. Early theoretical work by Falk and Arnett (1973) showed that hydrodynamical instabilities should appear in explosions of such massive stars. As the shock wave propagates through the stellar envelope it sets up density and pressure profiles which can in some cases result in the formation of Rayleigh-Taylor (RT) instabilities (Chevalier 1976). In particular, RT instabilities are expected to grow at the interface of the core and the hydrogen envelope because of the large entropy (and density) jump that occurs there (Weaver & Woosley 1980). A direct consequence of these instabilities is that chemical mixing in the ejecta takes place (Bandiera 1984).

Herant & Woosley (1994) have studied 2-D simulations of red supergiant explosions over a wide mass range, and found that the growth of hydrodynamic instabilities is highly likely in all cases. They showed that as the explosion (outgoing) shock plows into the hydrogen envelope, a reverse (ingoing) shock is formed, and between them, RT instabilities grow. Bubbles of hydrogen formed by these instabilities are violently dragged towards the centre of the star by the reverse shock. Simultaneously, compact helium and oxygen clumps advance out into the hydrogen envelope and bubbles of ^{56}Ni are formed and distributed in the outer parts of the ejecta. It has also been realised that strong dredge-up should result from the neutrino-driven convection close to the neutron star surface (Herant & Benz 1992) which has been invoked to account for the conversion of the core-collapse to explosion. This should also produce fast-moving blobs or “fingers” of radioactive material which eventually penetrate the outer layers of the supernova.

So far, only SN 1987A has provided us with clear observational evidence for dredge-up in a core-collapse event. This includes the shape of the light curve, the early detection of X-rays and γ -rays and the width of the iron lines in the infrared. However SN 1987A was, of course, only a single event, and a rather unusual one in that it arose from a blue supergiant progenitor. Therefore, we cannot simply assume that similar dredge-up occurs in all other type II events. Indeed, simulations have shown that differences in progenitor structure can lead to significantly modified hydrodynamical evolution (Herant & Benz 1992; Herant & Woosley 1994). Clearly, to establish whether or not deep dredge-up is typical of all core-collapse supernovae, a major step would be to demonstrate dredge-up and mixing in the most-common of all core-collapse events, the type IIp supernova.

A powerful demonstration of the occurrence of deep dredge-up would be the appearance of radioactive material at the surface at early times. Helium lines arising in the supernova envelope can be used as a tracer of the upwardly-mixed radioactive material. Helium lines are of high excitation. During the first week of the supernova, recombination maintains the populations of the excited levels and so He I lines are seen. However after about 10 days, the conditions in the type IIp atmosphere are such that all the helium will have recombined and de-excited to the ground state. But, if dredge-up oc-

curs during the explosion, radioactive ^{56}Ni may reach the outer parts of the supernova envelope at early times. If it does, the γ -rays from its decay ($^{56}\text{Ni} \Rightarrow ^{56}\text{Co} \Rightarrow ^{56}\text{Fe}$) will excite or re-ionise the helium. Thus the detection of helium lines during the plateau phase (20-120 d post explosion) should imply upward mixing of radioactive material from the core. Unfortunately no optical He I lines have ever been unambiguously identified during the plateau phase. However, there are two well-known strong lines in the infrared viz. He I 10830 Å ($2s^3S-2p^3P^0$) and 20580 Å ($2s^1S-2p^1P^0$) which offer the prospect of testing for dredge-up of radioactive material. This technique was applied by Graham (1988) and Chugai (1991) using the 10830 Å line in the SN 1987A at early times. Lucy (1991) invoked upward mixing of ^{56}Ni to account for strong optical He I lines in the early-time spectra of type Ib supernovae.

To investigate dredge-up in type IIp supernovae we began in 1995 a programme of infrared and optical spectroscopy of this type of supernova. The data we present here comprise an extensive set of IR/optical spectroscopic observations of the type IIp SN 1995V, spanning epochs of 22 to 85 days post explosion. The observations are described in section 2. In section 3 we compare the observations with a simple spectral synthesis model and discuss the line identifications, especially in the IR. In section 4 we describe the method we used to estimate the amount of dredge-up of ^{56}Ni . In section 5 we present the results from the comparison of the model with the data, and our estimations for the amount of dredge-up. In section 6 we discuss the implications of this work for our understanding of dredge-up.

2 Observations

SN 1995V was discovered in NGC 1087 on 1995 August 1 by R. Evans (1995). It lay 21" east and 3" south of the centre of its host galaxy. The unfiltered CCD magnitude of the supernova at discovery was +15 (Dopita & Trung Hua 1995) and strong P Cygni Balmer lines observed on August 2 (Benetti 1995) showed it to be a type II event near maximum light. Below, we deduce that to within a couple of days, the epoch of shock breakout was 1995 July 25. We adopt this as epoch 0 days and refer all other epochs to this fiducial date. Subsequent to its discovery, no broad-band photometry for SN 1995V was reported. However, we can be certain that it was a *plateau* type II event since the spectra exhibit a broad, well-developed absorption component at $\text{H}\alpha$ (Figure 1). This is generally absent from *linear* type IIs (Schlegel 1996). Identification of SN 1995V with a plateau type II event is confirmed by the evolution of the optical flux, as explained below.

2.1 Optical observations

The optical spectroscopy observations of SN 1995V were carried out using the Intermediate Dispersion Spectrograph (IDS) of the Isaac Newton Telescope (INT) on La Palma. Spectra were obtained on days 23, 34, 72 and 84 post-shock breakout (see

below). The optical spectroscopy log is given in Table 1.

The spectra were reduced by means of standard routines in the data-reduction package FIGARO (Shortridge 1991). The CCD frames were debiased, flat-fielded, and sky-subtracted. The spectra were extracted using the optimal-extraction algorithm of Horne (1986). Wavelength calibration was by means of CuNe and CuAr arc lamps. Feige 25 was the spectrophotometric flux standard. The optical spectra are presented in Figure 1. The fluxes shown in Figure 1 have been scaled as explained below.

Observing conditions were poor during most of the optical observations, and only on day 23 were conditions close to photometric. On this day, we judge the fluxing to be accurate to $\pm 15\%$. The fluxing for the other three epochs is less certain. Nevertheless, in order to confirm that SN 1995V was a type IIp event, we derived “BV magnitudes” from the optical spectra by multiplying them with the filter response functions B3 (also known as ϕ B) and V of Ažusienis & Straižys (1969). These magnitudes are presented in Table 2. Note that these magnitudes are uncorrected i.e. they were derived *before* application of the flux scaling corrections described below.

We then compared the B magnitudes with those of the type IIp SN 1983K (Phillips *et al.* 1990) (Figure 2). Unusually, this supernova was discovered before maximum light and so its time of shock break-out, t_0 , is known quite accurately. In Figure 2 it can be seen that, in spite of the fluxing uncertainties for SN 1995V, the B magnitudes show a similar evolution to those of SN 1983K during its plateau phase.

The horizontal displacement between the two light curves is constrained by the fact that SN 1995V was not detectable with a 0.41m reflector on 25 July 1995 (Evans, 1995). The similarity of the light curve shapes confirms that SN 1995V was indeed a plateau type II. From the comparison of the two light curves, we deduce that the time of the shock break-out, t_0 , for SN 1995V was 25 July 1995 ± 2 days.

2.2 Infrared observations

Infrared spectra were obtained at the Anglo-Australian Telescope (AAT), Siding Spring, using the Infrared Imaging Spectrograph, IRIS, and at the United Kingdom Infrared Telescope (UKIRT), Hawaii, using the Cooled Grating Spectrograph, CGS4. Spectra were obtained on days 22, 42, 44, 69 and 85. The IR spectroscopy log is given in Table 3.

Given the complexities of instrument scheduling on major telescopes, the match in epoch between the four optical and four IR spectra is remarkable. Note that these data are the first ever infrared spectra obtained of a type IIp during its photospheric phase. The IRIS spectra were reduced using FIGARO. The cross-dispersed spectral orders were first straightened. The frames were then flat-fielded and sky-line subtracted. The spectra were then optimally extracted. Wavelength calibration was performed by means of a CuAr arc, and the flux standard was HD 19904, assuming $J=6.727$. The CGS4 data were reduced using CGS4DR (Daly & Beard 1992) and FIGARO. A krypton arc

was used for wavelength calibration, and BS 770 and HD 18881 were the flux standards. The adopted magnitudes were $J=5.60$, $H=5.4$, $K=5.35$ for BS770 and $J=7.13$, $K=7.14$ for HD18881. The IR spectra are shown in Figure 3. The fluxes shown in Figure 3 have been scaled as explained below.

2.3 Flux calibration

Photometric conditions occurred for the IR observations on days 22 and 69, and so we judge the IR fluxing at these epochs to be better than $\pm 10\%$. However, for the other epochs the fluxing of the optical and IR spectra presented problems owing to both adverse weather conditions and technical difficulties during the observations. In order to improve the fluxing accuracy for those spectra taken under difficult conditions, we proceeded as follows. The day 72 optical spectrum was scaled so that the flux at the red end was consistent with that of the blue end of the well-fluxed day 69 IR spectrum, assuming a Rayleigh-Jeans slope in the small (360 \AA) gap between the optical and IR coverage. The scaled optical spectrum was then used to derive a corrected V magnitude using the method described above. A template V-band light curve was derived from the observations of the type IIp SNe 1969L (Ciatti, Rosino & Bertola 1971) and 1991G (Blanton *et al.* 1995). The SN 1995V day 72 corrected V magnitude was then used to set the template zero-point for this supernova, and the resulting light curve used to obtain the V magnitudes for days 23, 34 and 84. The optical spectra were then scaled to match these V magnitudes. For day 23 this spontaneously provided an excellent match to the well-fluxed day 22 IR spectrum in the overlap region, reinforcing our belief that the scaling procedure was valid. The lack of IR light curves for this type of supernova meant that a different approach was required to correct the IR fluxing on days 42, 44 and 85. Correction of the JH-band spectrum on day 44 was achieved using a linear interpolation of the IR fluxes between days 22 and 69, while the day 42 K-band spectrum was scaled to match the overlap with the corrected day 44 JH-spectrum. The day 85 IR spectrum was simply scaled to match the day 84 optical spectrum in the overlap region.

3 Line identifications

The optical spectra shown in Figure 1 are consistent with SN 1995V being a classic type IIp event. The $H\alpha$ P Cygni profile is strong throughout the plateau phase. Other prominent lines include $H\beta$, Na I-D (possibly blended with He I 5876 \AA) and the Ca II IR triplet. As SN 1995V evolved the absorption line profiles, especially those of $H\alpha$, $H\beta$ and the Ca II triplet, became narrower and deeper. The number of discernible lines increased with time so that by day 72 it was very difficult to determine the location of the continuum level in the B and V bands. As expected (Branch 1987; Elias *et al.* 1988), the IR spectra (Figure 3) have fewer features than in the optical region, but these also became more pronounced as the supernova evolved. Especially prominent is

a group of lines in the 10000–11200 Å range. In addition, Paschen lines and Br γ are all present. The identification of other IR lines is discussed below.

To investigate the spectra we used a simple spectral model where we assumed a spherical, homologously expanding envelope. We adopted a power law density profile, $\rho(r) = \rho(ph)(\frac{r}{r_{ph}})^{-n}$, where $\rho(ph)$, r_{ph} are the density at, and the radius of the photosphere respectively. The model continuum consisted of a dilute blackbody which incorporated the flux dilution (ζ) parameters specified by Eastman *et al.* (1996). The temperature was adjusted to match the observed continuum. The lines were formed in a pure-scattering atmosphere lying above the dilute blackbody photosphere (Castor 1970). For each transition, we assumed that the population of the upper level is negligible compared with that of the lower level. (Support for this assumption was provided by our detailed modelling of the He I 10830 Å line described below, where the lower level population was found to exceed that of the upper level by a factor of about 10^4). Line blending was treated using the formulae for doublet profiles described by Castor *et al.* (1979). For the line identifications, line IDs of Williams (1987), Elias *et al.* (1988), McGregor *et al.* (1988) and Meikle *et al.* (1989) and the predicted line strengths of Branch (1987) were taken into account. Transition wavelengths and oscillator strengths were taken from Kurutz (1996). The models were reddened using A_V calculated from the empirical wavelength dependence formula of Cardelli *et al.* (1989). The absolute visual extinction, $A_V=1.37\pm 0.11$, was estimated from the interstellar Na I-D lines, which were observable in all the optical spectra. This was done using the relation $E(B-V)\sim 0.25 EW(\text{Na I-D})$ which Barbon *et al.* (1990) derived from their supernova observations, together with an assumed $A_V=3\times E(B-V)$ (Whitford 1958). The model was also redshifted to match the recession velocity of NGC 1087, $v_0=1519\pm 6$ km/s (de Vaucouleurs *et al.* 1991).

For each line, the model’s free parameters were the population at the photosphere of the lower level of the transition, $N_{low}(ph)$, and the velocity at the photosphere, $v(ph)$. An additional free parameter was the density profile index, n , where the lower level population at radius r is given by: $N_{low}(r) = N_{low}(ph)(\frac{r}{r_{ph}})^{-n}$. At a given epoch, the weak metal lines, such as those of Fe II, Ba II and Sc II all tended to yield the same values for $v(ph)$ and n . In Table 4 we show these values. Their uncertainties are judged to be less than $\pm 10\%$. The constancy of $v(ph)$ amongst these lines at a particular epoch, together with their weakness, indicate that they were optically thin and that the derived velocities correspond to material at the true photosphere. For the optically-thin lines, we find that $v(ph)$ declined from 6200 km/s on day 22 to 2200 km/s on day 85. Compared with SN 1987A, SN 1995V presented higher photospheric velocities at comparable epochs. The density index obtained from the weak lines was then adopted for the model matches to the optically-thick lines. Significantly higher velocities were found for the prominent, strong lines of hydrogen and the calcium IR triplet and so we conclude that they were optically thick throughout the 22–85 day period.

The modelled and observed spectra are compared in Figures 4 (optical) and 5 (infrared). Line identifications, together with their individual values for $N_{low}(ph)$ and $v(ph)$, are presented in Tables 5 and 6. For optically thick lines, “ $v(ph)$ ” corresponds to the velocity at which the line became optically thick.

In the optical region, lines of neutral hydrogen, carbon, sodium and calcium, together with lines of singly-ionised carbon, calcium, scandium, iron, strontium and barium were identified. At later epochs, the matches to the data in the blue region are less satisfactory due to line blanketing. Consequently, the line identifications in this wavelength region on days 72 and 84 are less secure. The model also fails to reproduce the emission component of $H\alpha$. This effect has been known about for many years. It is explained by invoking collisional excitation from the $n=2$ to $n=3$ level which greatly enhances the emission component (e.g. Branch *et al.* 1981). A similar effect is not seen in the other Balmer lines since the line optical depths are such that, rather than escape, the line photons are more likely to be converted to $H\alpha$ plus a Paschen, Brackett etc line (Branch *et al.* 1981; Xu *et al.* 1992). This also adds to the $H\alpha$ emission.

The infrared spectra are largely dominated by the continuum. As indicated above, Paschen lines and Brackett γ are also present at all epochs. The other infrared lines include Sr II 10327 Å, Fe II 10547 Å, C I 10695 Å and He I 10830 Å. As can be seen from Figure 5 the model underproduces the emission components of the Paschen lines i.e. the IR hydrogen lines are clearly not formed by pure resonant scattering. Similar behaviour was observed in the early-time spectra of SN 1987A (e.g. Larson *et al.* 1987, Meikle *et al.* 1989) and is thought to be due to the conversion of Balmer line photons to $H\alpha$ plus Paschen, Brackett, etc line photons, as mentioned above.

Of special interest is the identification of the Sr II 10327 Å line. The line was also identified in the SN 1987A spectra (Elias *et al.* 1988) The presence of this line and of the Ba II lines indicates that s-process element enhancements might have occurred in the supernova progenitor (Williams 1987).

To double-check the He I 10830 Å identification we repeated the model fit but with the helium line excluded. The result is shown in Figure 6. Clearly the no-helium model provides a much inferior match to the data. We conclude that He I 10830 Å was definitely present on days 69 and 85. *We believe that this is the first time that helium has been clearly identified in a type IIp supernova during the plateau phase.* The velocity at the He I 10830 Å “photosphere” declined from 4250 km/s to 3750 km/s between days 69 and 85. This is substantially higher than the corresponding photospheric velocities of the weak lines and even those of the Balmer lines (apart from $H\alpha$), indicating that the helium was optically thick. The absence of He I 20580 Å does not cast doubt upon the He I 10830 Å identification since our model indicates that the He I 20580 Å line is at least a factor of 100 weaker.

4 Investigation of ^{56}Ni dredge-up using the He I 10830 Å line.

The He I 10830 Å ($2s^3S-2p^3P^0$) line is formed in a region where the population of the metastable $2s^3S$ level is maintained by the balance of the recombination rate of He^+ with the rates of collisional de-excitation and forbidden radiative decay (Elias *et al.*

1988). However, because the He^+ recombination time scale is < 1 d (Graham 1988) we expect that at the times observed (69d-85d) all helium should be neutral and in its ground state. The persistence of the He I line at such late times requires an increasing ionisation rate to raise the electron density faster than it is diluted by the expansion. Following Graham (1988), to account for the persistence of the He I line, we propose that the ionisation is maintained by the decay of ^{56}Co which resulted from the decay of ^{56}Ni produced in the explosion. The decay γ -rays and resultant Compton-scattered electrons re-ionize the helium. The subsequent recombination produces the observed He I 10830 Å line.

To explore the radioactive decay scenario, we calculate the radioactive energy deposited in the outer envelope of the supernova and hence find the ionisation balance as a function of radius. We then determine the $2s^3S$ population density profile. This is then used to replace the $2s^3S$ power-law profile in the P Cygni models described above and the calculated spectrum compared with the observations. We first applied this technique using a specific explosion model, s15s7b2f (Weaver & Woosley 1993). We considered two cases *viz.* one in which the helium in the envelope is entirely microscopically mixed with the hydrogen (i.e. 100% primordial H/He), and one in which various fractions of the helium in the envelope are clumped. As will be explained below, the presence of clumps of unmixed helium above the photosphere can dramatically reduce the required degree of ^{56}Ni dredge-up. However, it will be shown that even for the clumped-helium case, model s15s7b2f does not reproduce the He I 10830 Å line. We then modified model s15s7b2f by increasing the extent of the dredge-up of ^{56}Ni to produce a match to the observations. Again, we consider cases where helium is unclumped and clumped.

The decay of ^{56}Ni and ^{56}Co produces a number of ~ 1 MeV γ -ray lines of different energies. The energy is deposited in the expanding envelope via Compton-scattering. The differential scattering cross-section and the fractional energy transfer are highly dependent upon the scattering angle. Moreover, the high-energy electrons produced by the Compton scattering go through many interactions with ions and electrons before finally yielding up the last of their energy (Sutherland & Wheeler 1984). Ideally, such a process should be modelled using a Monte Carlo simulation in order to compute the rate at which the high energy electrons transfer their energy to the environment. However, Monte Carlo techniques are excessively demanding of computational resources. For this initial study, therefore, instead of attempting a Monte Carlo analysis, we adopted the “gray” approximation of Sutherland and Wheeler (1984). In their method, they assume a purely absorptive γ -ray opacity, κ_γ , which is independent of the energy of the γ -rays. The value they adopt, $\kappa_\gamma=0.03 \text{ cm}^2\text{g}^{-1}$, is in accord with that based upon Monte Carlo simulations (Colgate *et al.* 1980, Sutherland & Wheeler 1984, Swartz *et al.* 1995). The details of the deposition calculation are included in the Appendix.

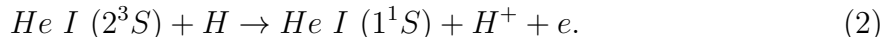
In a H/He envelope of low ionisation, all the energy produced by the Compton scattering of the γ -rays is deposited in the H and He causing ionisation, rather than in the heating of the electron gas (Meyerott 1980). Therefore, for a deposition rate of ϵ_i in species i the abundance of the next ionisation stage $i+1$ is given by the energy balance :

$$n_{i+1} = \frac{\epsilon_i}{n_e \alpha_i w_i} \quad (1)$$

where n_e is the electron density ($n_e = n_{He\ II} + n_{H\ I}$), α_i is the recombination rate to all levels of the species i and w_i is the energy required to produce an ion-electron pair. The ratio of energy deposited in H and He is $\epsilon_{He}/\epsilon_H = mY$, where $Y = n_{He}/n_H$. From the Bethe-Bloch formula for energy loss of fast electrons in H/He material, we find m to be 1.7.

Our model includes the detailed effect of the fast electrons on the populations of excited states of He I. We ignore direct excitation since the fast electrons excite only singlet states, which decay rapidly back to the ground state. The key populating process is recombination. Of the recombinations to excited levels of He I, approximately three-quarters are to triplet states, with the remainder going to singlet states (Osterbrock 1989). Recombinations to singlet levels ultimately populate the $2s^1S$ and $2p^1P$ levels. Atoms in the $2p^1P$ state decay mostly to $1s^1S$ but some may also decay to $2s^1S$. However the $1s^1S$ - $2p^1P$ transition is highly optically thick with the result that all the singlet recombinations eventually pass through the $2s^1S$ state. Atoms in $2s^1S$ level decay by two-photon emission ($A=51\text{ s}^{-1}$) to the ground state. Thus, only a small population of excited singlet states is built up and consequently the optical depths of absorption lines arising from excited singlet levels are small.

All captures to triplet levels lead, through downward radiative transitions, to the highly metastable $2s^3S$ level where the population can become quite substantial. There are a number of mechanisms which can depopulate this level. Two, purely radiative, depopulating mechanisms can be identified. A very weak single-photon radiative decay to $1s^1S$ can occur ($A=1.27\times 10^{-4}\text{ s}^{-1}$) (Osterbrock 1989). Of considerably greater significance, however, is the 2-stage intersystem radiative decay $2s^3S\rightarrow 2p^3P\rightarrow 1s^1S$. This occurs in the presence of a radiation field (such as from the photosphere), which is required to excite the first stage. There are also two important depopulating processes involving collisions. One of these simply involves thermal electron collisions causing excitation or de-excitation from $2s^3S$ across to singlet states. The other process is Penning ionisation (Bell 1970, Chugai 1991):



This process requires microscopic mixing of hydrogen and helium but in the event of such mixing, it dominates the depopulation of the $2s^3S$ level (see below).

We can therefore summarise the population balance of the $2s^3S$ level with the equation:

$$n_{He(2^3S)}(n_e Q + C_P + R + A) = \alpha(n^3 L)n_e n_{He\ II}. \quad (3)$$

Q is the sum of the collision rates from $2s^3S$ to all singlet states, and has the value $1.826\times 10^{-8}\text{ cm}^3\text{ s}^{-1}$ (Berrington & Kingston 1987). C_P is the Penning ionisation rate and is given by $C_P = \gamma_P n_H$ where $\gamma_P = 7.5 \times 10^{-10} (\frac{T}{300K})^{1/2}\text{ cm}^3\text{ s}^{-1}$ (Bell 1970, Kozma 1996). For the recombination temperature of hydrogen ($T\sim 5000\text{ K}$), which we adopted for the days concerned (plateau phase), $\gamma_P=3\times 10^{-9}\text{ cm}^3\text{ s}^{-1}$. $A = 1.27\times 10^{-4}\text{ s}^{-1}$, is the

A-value for the single-photon radiative decay to $1s^1S$. $\alpha(n^3L) = 3.26 \times 10^{-13} \text{cm}^3 \text{s}^{-1}$ is the total recombination coefficient for the triplet states at a temperature of 5000 K (Osterbrock 1989). R is the two stage inter-system radiative decay rate (Chugai 1991). This is given by:

$$R = B_{23} \frac{4\pi}{c} \left(\frac{D}{vt}\right)^2 F_\nu^C e^{0.92A(\lambda)} A_{32}^{-1} A_{31} \beta_{31} \quad (4)$$

where β_{31} is the escape probability for the photon emitted in the decay $2p^3P \rightarrow 1s^1S$ and F_ν^C is the flux of the continuum at $\lambda=10830 \text{ \AA}$, determined from the observed infrared spectra. $A(\lambda)$ is the extinction calculated using the empirical formula by Cardelli *et al.* 1989 (*cf.* Section 3). For the distance D , a value of 16.7 Mpc was derived from the infall model described in Aaronson *et al.* 1982. v is the velocity at the He I “photosphere” at time t (*cf.* Table 6)

As mentioned above, the population balance is extremely sensitive to the effects of Penning ionisation. This is illustrated in Table 7 where we compare the $2s^3S$ depopulation rates in microscopically mixed H/He for the different mechanisms. The rates were calculated for $n_e \sim 10^6 \text{cm}^{-3}$, $n_H \sim 3 \times 10^{10} \text{cm}^{-3}$ and $n_{He} \sim 4 \times 10^9 \text{cm}^{-3}$, which are typical for the He I 10830 \AA line-formation region at the epochs concerned ($t \sim 60\text{-}80$ days). We see that Penning ionisation dominates the depopulation of the $2s^3S$ level. Thus, for typical conditions, any helium that is intimately mixed with hydrogen will have its $2s^3S$ state so heavily depopulated that its contribution to the $2s^3S$ population in the envelope will be negligible. Putting it another way, pure helium clumps above the $2s^3S$ photosphere, such as might be produced by RT instabilities at the H/He interface, will tend to dominate the $2s^3S$ population. Helium that is microscopically mixed with hydrogen, such as primordial helium, will make a negligible contribution even if its abundance is much greater. Thus, the ^{56}Ni -driven ionisation rate inferred from the He I 10830 \AA data depends on what fraction of the helium in the envelope is clumped and what fraction is intimately mixed with the hydrogen. The greater the microscopic mixing, the greater must be the ^{56}Ni -driven ionisation rate to produce the observed He I 10830 \AA . Although it is likely that RT instabilities at the H/He interface will mix some clumps of helium up into the hydrogen layer (Herant & Woosley 1994), unfortunately the actual fraction of clumped helium in the envelope is unknown. We therefore examine two cases - one involving no clumps of pure helium, and one involving two different degrees of helium clumping.

4.1 He I 10830 \AA line strength predictions from s15s7b2f explosion model

4.1.1 Case 1: Hydrogen and helium 100% microscopically mixed

In this case the He I 10830 \AA line is formed entirely by microscopically mixed (primordial) helium, and so the dominant mechanism for the depopulation of the $2s^3S$ level is Penning ionisation. Equations (1) therefore reduce to :

$$\frac{\epsilon_H}{w_H} + n_{He(2^3S)}n_{H\ I}C_P = n_{HII}n_e\alpha_{H\ I} \quad (5)$$

$$\frac{\epsilon_{He}}{w_{He}} = n_{He\ II}n_e\alpha_{He} \quad (6)$$

where $\epsilon = \epsilon_{He} + \epsilon_H$ is the energy deposited in the envelope. From the Bethe-Bloch formula $\epsilon_{He}/\epsilon_H = mY$, and assuming $n_e = n_{HeII} + n_{HII}$ we can calculate the population of the $2s^3S$ level, $n_{2s^3S}(R)$ as a function of radius, R , using equations (5) and (6). This requires the energy deposition rate $\epsilon(R)$, the total number density $n_{tot}(R) = n_{He\ I}(R) + n_{H\ I}(R) + n_e(R)$, and the relative abundance of hydrogen and helium, $Y = \frac{n_{HeII}(R) + n_{HeI}(R)}{n_{HII}(R) + n_{HI}(R)}$. The last two quantities were obtained from explosion model s15s7b2f.

In this model, a $15 M_\odot$ progenitor is exploded, ejecting $0.0643 M_\odot$ of ^{56}Ni . The density profile of the ^{56}Ni goes to zero at 750 km/s from the core. Using this density profile we calculated the deposition rate $\epsilon(R)$, using the formula of Sutherland & Wheeler (1984) as described in the Appendix. The calculated density profile of the population of the $2s^3S$ level, $n_{2s^3S}(R)$, was then fed into the P Cygni models for days 69 and 85. These are presented in Figure 7 compared with the observations. Clearly the contribution of He I 10830 Å to the model spectrum is negligible (*cf.* Figure 6). We deduce that the ^{56}Ni density profile specified by model s15s7b2f is inadequate to account for the observed He I $2s^3S$ population if 100% microscopic mixing of the helium and hydrogen is assumed.

4.1.2 Case 2: Clumps of helium in the hydrogen envelope

If clumps of “pure” helium exist in the hydrogen envelope then, as explained above, the observed He I 10830 Å line will be formed almost entirely by the clumped helium since depopulation of $2s^3S$ by Penning ionisation will not affect such regions. We investigated the effect of helium clumping by assuming that a certain fraction of the helium mass in a region was in the form of clumps *i.e.* unmixed with hydrogen. The exclusion of the Penning mechanism in this case meant the main de-populating mechanisms were 2-stage intersystem radiative decay and collisional depopulation. In order to calculate the effects of these processes on the $2s^3S$ population it was necessary to use a more detailed helium model consisting of the ground state $1s^1S$ and the first four excited states. The processes considered in our model included recombination, collisional excitations and de-excitations, radiative decays (allowing for the escape probability of the line photons), and the two-stage radiative transition $2s^3S \rightarrow 2p^3P \rightarrow 1s^1S$ for the depopulation of the $2s^3S$ level. Energy levels and empirical formulae for collision strengths were provided by Berrington & Kingston (1987) for $T=5000$ K. Radiative decay rates were provided by Mendoza (1983) and recombination coefficients for each level were obtained from Osterbrock (1989).

The electron density in the clumps was estimated from the balance between ionisations

and recombinations:

$$\frac{\epsilon^{clumps}}{\omega_{He}} = n_{He\ II}^{clumps} n_e^{clumps} \alpha_{He} \quad (7)$$

where ϵ^{clumps} is the energy deposited per sec per cm^3 in the clumps, ω_{He} is the energy required to produce an ion pair, and α_{He} is the recombination coefficient for He^+ . Because the clumps consist of pure helium, it follows that $n_e^{clumps} = n_{He^+}^{clumps}$. We can therefore estimate the electron density in the clumps using equation (7), provided we know the energy deposited there.

As explained in the Appendix, the energy per sec per cm^3 that is deposited in a region is proportional to the density of the region *i.e.* $\epsilon \propto \rho$. We envisage that the pure helium clumps are in pressure balance with a surrounding envelope which has the primordial H/He abundance ratio. Consequently we have:

$$P_{clumps} = P_{env.} \implies \frac{\rho_{clumps} N_{Av} k T}{\mu_{He}} = \frac{\rho_{env.} N_{Av} k T}{\mu_{env}} \implies \rho_{clumps} = \rho_{env.} \frac{\mu_{He}}{\mu_{env}} \quad (8)$$

where N_{Av} is Avogadro's number, k is Boltzmann's constant, and μ_{env} , μ_{He} are the mean molecular weight of the envelope gas and the helium clumps respectively. The mean molecular weight of the mostly neutral gas in the He I line-forming region is given by: $\mu_{env} \approx (\frac{X_H}{1} + \frac{X'_{He}}{4} + \frac{X_Z}{2})^{-1}$ where X_H , X'_{He} , X_Z are the abundances of the hydrogen, primordial helium, and metals in the envelope gas. We assumed that a certain fraction, χ_{He} , of the total helium mass is clumped *i.e.* unmixed with hydrogen. Therefore the residual primordial helium abundance, X'_{He} , becomes: $X'_{He} = X_{He} - (\chi_{He} X_{He})$, where X_{He} is the average helium abundance in the zone considered. The radial profiles of the abundances X_H , X_{He} , X_Z were obtained from the s15s7b2f explosion model. In practice, X_Z was small and so was omitted from the calculation.

Using equation (8) with $\chi_{He}=0.5$, we calculated the corresponding clump densities and then calculated the energy deposited there. We then determined the $2s^3S$ level population in the clumps using the five-level helium atom model described above. The calculated population profile, $n_{2s^3S}(R)$, was fed into the P Cygni model and the resulting model spectra compared with the observations. These are presented in Figure 7. In spite of the fact that the clumped helium is unaffected by Penning ionisation, we still find that the He I 10830 Å makes a negligible contribution to the model spectrum, even for χ_{He} as high as 0.5. We conclude that even by invoking clumped helium, explosion model s15s7b2f is still unable to yield sufficiently high $2s^3S$ level populations to account for the observed helium line. Given that ^{56}Ni only extends to 750 km/s in model s15s7b2f, this failure is not surprising since, for example, at 69 days the helium photosphere is at 4250 km/s. The gamma-rays simply do not penetrate to sufficiently high velocities. *We conclude that the radial extent of ^{56}Ni must be greater than specified by model s15s7b2f.*

4.2 He I 10830 Å line strength predictions from model s15s7b2f plus additional ^{56}Ni dredge-up

We propose that the persistence of the He I 10830 Å line is due to the upward mixing of ^{56}Co into the outer layers of the supernova envelope. A similar proposal was made by Graham (1988) for the peculiar type II SN 1987A. To investigate the extent of this upward mixing, we have modified the s15s7b2f model results so as to place radioactive nickel beyond 750 km/s.

To do this, we invoked a ^{56}Ni density profile in which the density remained constant up to velocity v_c and then declined as a power law of index k (Figure 8). The total ^{56}Ni mass was always held at the s15s7b2f value *viz.* $0.0643 M_\odot$. v_c and k are free parameters. The density profiles for other elements in s15s7b2f were unchanged. In each zone the nickel was homogeneously mixed with the other elements. We then proceeded as before to calculate the $2s^3\text{S}$ population profile. This was then applied to the P Cygni model and the model spectrum compared with the observations. k and v_c were adjusted to provide simultaneous matches to the observed spectra on days 69 and 85. As before, we considered cases where the helium was unclumped or clumped. The ranges of values for v_c and k which provided good matches are shown in Table 8, and examples of corresponding ^{56}Ni profiles are shown in Figure 9. An example of the synthetic spectra produced using the values $\chi_{\text{He}}=0.1$, $k=9$, $v_c=800\text{km/s}$ is shown in Figure 10.

Clearly, with sufficient upward mixing of the ^{56}Ni , the modified s15s7b2f model is able to reproduce the He I 10830 Å emission. We note that in the case of clumped helium, v_c has roughly the same value as the ^{56}Ni boundary in model s15s7b2f *viz.* ~ 750 km/s. However, for the case where the helium is entirely microscopically mixed with the hydrogen we find, unsurprisingly, that v_c must extend much further *viz.* to ~ 1150 km/s. In the power law zone, we find an index of about 8 or 9 for all the cases considered. For each case, we calculated the ^{56}Ni mass in the power law zone, and the mass above the helium photosphere. These are presented in Table 8. In all cases, we see that about a third of the total ^{56}Ni mass must have been dredged up beyond the v_c limit. The larger v_c in the no-clumped helium case implies a considerably greater dredge-up. Dramatically different masses of ^{56}Ni above the He I photosphere are inferred for the clumped and no-clumped cases, with a factor of ~ 30 more ^{56}Ni being required for pure microscopic mixing, relative to 10% clumping.

5 Discussion

Reproduction by explosion model s15s7b2f of the observed He I emission is achieved only by invoking substantial additional dredge-up of the ^{56}Ni from the core. As expected, the case with no helium clumping requires the greatest dredge-up. However, we argue that the no-clumping case is probably highly unrealistic, since it is difficult to see how one could achieve such a large amount of ^{56}Ni dredge-up and yet have no pure

helium clumps in the same environment. We deduce, therefore, that there must exist some pure helium clumps in the hydrogen envelope. As we have shown, with fairly modest clumping of $\chi_{He} = 0.1$ or 0.2 , the uniform central core coincides, to within the errors with that of the unmodified s15s7b2f model. The addition of a steep, power-law density component to this will bring sufficient ^{56}Ni to the surface to account for the He I 10830 Å emission. Nevertheless, the fraction of the ^{56}Ni mass which must be dredged up beyond the uniform core is quite substantial. For SN 1995V we conclude that a) a small amount of ^{56}Ni ($\sim 10^{-6} M_{\odot}$) must have been dredged up to the helium photosphere ($v \sim 4,250$ km/s), and b) clumps of pure helium must have also existed in this region.

High velocities for the decay products of ^{56}Ni (~ 3000 km/s) were also observed in the ejecta of SN 1987A (e.g. Meikle et al. 1993). As shown by Herant & Benz (1992), if the ^{56}Ni is located at the base of the ejecta at $t \sim 300$ s it is impossible to accelerate even a small fraction to about 3000 km/s during subsequent instabilities. In order to achieve such high velocities, it is necessary to invoke outward mixing of the nickel at even earlier times, such as might be caused by neutrino convection. If this occurred, then the later instabilities would carry the nickel to still higher velocities. In order to match the observations of SN1987A, Herant & Benz had to premix nickel out to $1.5 M_{\odot}$ above the mass cut.

Herant & Woosley (1994) studied shock propagation, mixing and clumping in the explosion of red supergiants. In order to take into account the pre-mixing of ^{56}Ni during the initiation of the explosion, they diluted the nickel by a factor ~ 4 above the mass cut. They then followed the shock propagation and the growth of RT instabilities. For all progenitors their simulations showed that extensive RT instabilities develop in the ejecta in the wake of the reverse shock from the H/He interface. In contrast to the blue supergiant studies, these instabilities have ample time in which to evolve and completely reshape the ejecta. In spite of this, in all the explosions simulated, nickel did not reach velocities higher than ~ 1500 km/s. Similarly, helium did not exceed velocities higher than 2500 km/s. Our results, therefore, indicate that a higher degree of pre-mixing may be required than is invoked in the Herant & Woosley models.

Recently, Bazan & Arnett (1997) have simulated mixing in core-collapse events. Their simulations include both RT and Richtmeyer-Meshkov instabilities. These produce much higher velocities for ^{56}Ni than do R-T instabilities alone. Velocities as high as ~ 4000 km/s are predicted. The mass and profile index of the upwardly-mixed ^{56}Ni derived above could be of considerable value in constraining the initial parameters of these instabilities.

6 Conclusions

He I 10830 Å has been clearly identified in the infrared spectra of SN 1995V during the plateau phase. The velocity of the helium “photosphere” derived from this line declined from 4250 km/s to 3750 km/s between days 69 and 85. This was substantially

higher than the corresponding velocities of the metal lines and even of the Balmer lines indicating that helium was optically thick. The presence of the He I line at such late times suggests re-ionisation driven by the decay of ^{56}Co .

Using explosion model s15s7b2f we were unable to reproduce the observed He I line. However, with the additional upward mixing (dredge-up) of $\sim 10^{-6} M_{\odot}$ of ^{56}Ni to high velocities we were able to match the observed spectra. We also deduce that the He I line-forming region took the form of clumps of pure helium in the hydrogen envelope. We note that these deductions are insensitive to the accuracy of the flux calibration since they are based primarily on the optical depth of the He I P Cygni line. We conclude that the He I 10830 Å line can be used as a valuable probe for the study of mixing in a type II supernova. The next stage will be to extend this study to provide constraints on the size of the initial perturbations in mixing models.

Acknowledgements: We thank Brian Schmidt for helpful discussions, and in particular for originally pointing out to us the need for infrared spectroscopy of type IIp supernovae in the plateau phase. We also thank Stan Woosley for his advice and for the use of his explosion model. We are also grateful to Ron Eastman, Marcos Montes and Phil Pinto for useful discussions. We thank Charlene Heisler and Mike Irwin for carrying out some of the observations. AF is supported by a scholarship from the Alexander S Onassis Public Benefit Foundation. Much of the data reported here were obtained via the AAO, ING and UKIRT Service Programmes.

References

- Aaronson M., Huchra J., Mould J., Schechter P.L., Tully R.B., 1982, *ApJ*, **258**, 64
- Ažusienis A., Straizys V., 1969, *Soviet Astr.*, **13**, 316
- Ambwani K., Sutherland P., 1988, *ApJ*, **325**, 820
- Bandiera R., 1984, *A&A*, **139**, 368
- Barbon R., Benetti S., Rosino L., Cappellaro E., Turatto M., 1990, *A&A*, **237**, 79B
- Bazan G., Arnett, D., 1998 *ApJ*, **496**, 316
- Bell K.L., 1970, *J.Phys.B:Atom.Molec.Phys.* **3**, 1308
- Benetti S., 1995, IAU Circ.6197
- Berrington K. A., Kingston A. E. 1987, *J. Phys. B: At. Mol. Phys.*, **20**, 6631
- Blanton E.L., Schmidt B.P., Kirshner R.P., Ford C.H., Chromey F.R., Herbst W., 1995, *AJ*, **110**, 2868
- Branch B., Falk S.W., McCall M.L., Rybski P., Uomoto A.K, Wills B.J., 1981, *ApJ*, **244**, 780
- Branch D., 1987, *ApJ*, **320**, L121
- Cardelli J., Clayton G., Maths J., 1989, *ApJ*, **345**, 245
- Castor J.I., 1970, *MNRAS*, **149**, 111
- Castor J.I., 1979, *ApJS*, **49**, 481
- Chevalier R.A., 1976, *ApJ*, **207**, 872
- Ciatti F., Rosino L., Bertola F., 1971, *Mem.Soc.Astrom.Ital*, **42**, 163
- Chugai N.N., 1991, in *Supernovae*, ed. Woosley S.E., Springer-Verlay, New York, p286
- Colgate S.A., Petschek A.G., Kriese J.T., 1980, *ApJ*, **237**, L81
- Daly P.N., Beard S.M., 1992, *Starlink User Note* 27.1
- De Vaucouleurs G., De Vaucouleurs A., Corwin JR. H. G., Buta R. J., Paturel G., Fouquet E., 1991, *Third Reference Catalogue of Bright Galaxies*, Version 3.9
- Dopita M., Trung H.C., 1995, IAU Circ.6197
- Eastman R.G., Schmidt B.P., Kirshner R.P., 1996, *ApJ*, **466**, 911
- Elias J.H., Gregory B., Phillips M.M., Williams R.E., Graham J.R., Meikle W.P.S., Schwartz R.D., Wilking B., 1988, *ApJ*, **331**, L9
- Evans R.O., 1995, IAU Circ.6197
- Falk S.W., Arnett D.W., 1973, *ApJ*, **180**, L65
- Graham J.R., 1988, *ApJ*, **335**, L53
- Herant M., Woosley S.E., 1994, *ApJ*, **425**, 814
- Herant M., Benz W., 1992, *ApJ*, **387**, 294
- Horne K., 1986, *PASP*, **98**, 609
- Kozma C., 1996, PhD Thesis, Department of Astronomy, Stockholm University
- Kurutz R.L., 1996, *Atomic spectral line database*,
<http://cfa-www.harvard.edu/amp/data/kur23/sekur.html>
- Larson P.H., Drapatz S., Mumma M.J., *ESO Conference and Workshop Proceedings* No26 1987, 147
- Lucy L.B., 1991, *ApJ*, **383**, 308
- Meikle W.P.S., Allen D.A., Spyromilio J., Varani G.-F., 1989, *MNRAS*, **238**, 193
- Meikle W.P.S., Spyromilio J., Allen D.A., Varani G.-F., Cumming R.J., 1993, *MNRAS*, **261**, 535
- Mendoza C., 1983, in *Planetary Nebulae*, ed. Flower D.R., p143

Meyerot R.E., 1980, in Supernovae Spectra, ed. R.E. Meyerott and G.H. Gillespie (AIP Conf. Proc. 63), p49
McGregor P., 1988 Elizabeth and Frederick White Conference on Supernova 1987A, Canberra 1988, June 20-24, Proc.astr. Soc. Aust. 7,450
Osterbrock D.E., 1989, in Astrophysics of Gaseous Nebulae and Active Galactic Nuclei, p25
Philips M.M., Hamuy M., Maza J., Ruiz T., Carney B.W., Graham J.A., 1990, *PASP*, **102**, 299
Schlegel E.M., 1996, *AJ*, **111**, 1660
Shortidge K., FIGARO General data reduction and Analysis Styarlink MUD, RAL, June 1991
Sutherland P.G., Wheeler J.C., 1984, *ApJ*, **280**, 282
Swartz D.A., Sutherland P.G., Harkness R.P., 1995, *ApJ*, **446**, 766
Weaver T.A., Woosley S.E., 1980, in AIP Conf. Proc. 63 ,Supernovae spectra, ed R.Meyerott, G.H. Gillespie (New York: AIP), 15
Weaver T.A., Woosley S.E., 1993, Phys. Rep.**227**, 65
Whitford A.E., 1958, *AJ*, **63**, 201
Williams R.E., 1987, *ApJ*, **320**, L117
Xu Y., McCray R., Oliva E., Randich S., 1992, *ApJ*, **386**, 181

Appendix: Calculation of the deposition energy

Our calculation of the γ -ray deposition function is based on the formula described by Sutherland & Wheeler (1984). The formula is basically an absorption calculation which assumes that the γ -ray opacity, κ_γ , is independent of energy and totally absorptive. The value adopted, $\kappa_\gamma = 0.03 \text{cm}^2 \text{g}^{-1}$, is in accord with that based upon Monte Carlo simulations (Colgate *et al.* 1980, Sutherland & Wheeler 1984, Swartz *et al.* 1995).

The geometrical aspects of the absorption calculation were treated as follows. Consider an arbitrary point A in the ejecta, of mass $dm = \rho dA dl$, where dA is an infinitesimal area normal to the direction to a source of γ -rays at some other point. Then the rate of the energy deposited at this point due to the source is:

$$ds_{dep} = \kappa_\gamma \rho dl \frac{dA}{4\pi R^2} e^{-\tau(\mathbf{r})} s(\mathbf{r}) \quad (9)$$

where we take dm to be the origin of the co-ordinates, and the source at \mathbf{r} , emitting γ -ray energy at the rate $s(\mathbf{r})$ ergs $\text{g}_{rad}^{-1} \text{s}^{-1}$. The source $s(\mathbf{r})$ is spatially constant but it varies with time due to the exponential decay of the daughter nuclei. The total rate of the deposition function is given by the dimensionless deposition function da obtained by dividing ds_{dep} by dm and $s(\mathbf{r}) = \text{constant}$ and by integrating over the radioactive source region. Therefore we have:

$$d\alpha = \frac{\kappa_\gamma}{4\pi} \int d^3r \frac{1}{r^2} e^{-\tau(\mathbf{r})} \rho_{rad}(\mathbf{r}) \quad (10)$$

where $\rho_{rad}(\mathbf{r})$ is the density of the radioactive material and $\tau(\mathbf{r})$ is the optical depth,

$$\tau(\mathbf{r}) = \int_0^{\mathbf{r}} \kappa_\gamma \rho(\mathbf{s}) d\mathbf{s} \quad (11)$$

ρ is the total density. Assuming spherical symmetry equation (10) becomes:

$$\begin{aligned} da &= \frac{\kappa_\gamma}{2} \int d\mu \int dr \exp[-\tau(r)] \rho_{rad}(r) \Rightarrow \\ da(r_A) &= \frac{1}{2} \int d\mu \int_A^C \exp[-\tau] f_{rad}(r) \rho \kappa_\gamma dr = \\ &= \frac{1}{2} \int d\mu \int_A^C d\tau f_{rad}(r) \exp[-\tau] \end{aligned} \quad (12)$$

where $f_{rad}(r)$ is the fraction of the ^{56}Ni mass relative to the total mass and $\mu = \cos\theta$ (*cf.* Figure A). For the calculation of the dimensionless deposition function da we used the density profile of the s15s7b2f explosion model (Weaver & Woosley 1993). The model is divided in shells within each of which the density and the initial mass fraction of nickel, f_{rad} are constant. Equation (12) can then be integrated exactly (*cf.* Figure A)

$$da(r_A) = \int d\mu \left(\int_A^{B_1} d\tau f_{rad}(AB_1) \exp[-\tau] + \right.$$

Table 1: Log of optical spectroscopy of SN 1995V

Date UT 1995	Epoch (d)	Telescope/Instrument	$\lambda\lambda(\text{\AA})$	$\Delta\lambda(\text{\AA})^\alpha$	Slit (arcsec)
Aug 17.2	23	INT/IDS	3994-9256	6.5	1.5
Aug 28.2	34	INT/IDS	4165-9283	6.5	1.4
Oct 4.1	72	INT/IDS	3700-9522	6.2	1.5
Oct 16.1	84	INT/IDS	3950-9250	6.3	1.6

^αSpectral resolution.

Table 2: Uncorrected B and V magnitudes derived from the spectra of SN 1995V

Epoch (d)	B	V
23	16.45	15.86
34	16.70	15.80
72	17.20	15.84
84	17.47	16.24

Table 3: Log of infrared spectroscopy of SN 1995V

Date UT 1995	Epoch (d)	Telescope/Instrument	$\lambda\lambda(\text{\AA})$	$\Delta\lambda(\text{\AA})^\alpha$	Slit (arcsec)
Aug 15.8	22	AAT/IRIS	8416-15149	20.7	1.4
Sep 4.6	42	UKIRT/CGS4	18766-25427	25	1.2
Sep 6.6	44	UKIRT/CGS4	9988-13365 & 14400-21122	13.5 & 26.5	2.4
Oct 1.6	69	UKIRT/CGS4	9820-13310 & 18800-25373	13.5 & 27.5	2.4
Oct 17	85	AAT/IRIS	8441-15150	22	1.4

^αSpectral resolution.

Table 4: Model parameters giving the best reproduction of the observed infrared and optical spectra (optically thin lines only).

Epoch (d)	$v(\text{ph})$ (km/s)	n
22-23	6200	-5.1
44-34	3700	-4.5
69-72	2600	-3.0
85-84	2200	-3.0

Table 5: Line identifications and derived velocities, $v(\text{ph})$, (km/s) and lower level populations, $N_{\text{low}}(\text{ph})$, (cm^{-3}) for the optical spectra

Line	23 days		34 days		72 days		84 days	
	$v(\text{ph})$	$N_{\text{low}}(\text{ph})$	$v(\text{ph})$	$N_{\text{low}}(\text{ph})$	$v(\text{ph})$	$N_{\text{low}}(\text{ph})$	$v(\text{ph})$	$N_{\text{low}}(\text{ph})$
Sr II 4077	-	-	-	-	2850	1.1	2450	0.7
H δ	-	-	-	-	3100	0.6	2800	1.1
Ca I 4142	-	-	-	-	2600	0.7	2200	0.4
Ba II 4166	-	-	-	-	2600	3.5	2200	3.0
Fe II 4205	-	-	-	-	2600	8.5	2200	7.5
Sr II 4215	-	-	-	-	2500	0.2	2200	0.22
Ca II 4226	-	-	3700	0.34	2500	0.23	2200	0.22
Ca II 4289	-	-	4100	0.95	2600	0.6	2200	0.5
H γ	7100	17.5	5350	16.5	3100	13.5	2800	8.5
Ca I 4355	-	-	4000	15.5	2600	1.6	2200	1.3
Sc II 4400	-	-	-	-	2600	7.5	2200	10.0
Ca I 4425	-	-	-	-	2600	10.1	2200	9.0
Ba II 4524	-	-	3850	1.8	2600	1.25	2200	0.9
Ba II 4554	6400	1.3	3850	2.0	2600	1.12	2200	0.9
Ca I 4578	-	-	-	-	2600	5	2200	3
Ca I 4581	-	-	-	-	2600	1.33	2200	1.9
Ca I 4585	-	-	-	-	2600	0.28	2200	0.3
C II 4627	-	-	-	-	2500	12.3	2100	7
Sc II 4670	-	-	-	-	2700	3	2200	8
H β	7000	8	5100	6.6	3500	3.5	2900	2.05
Ba II 4934	-	-	4800	1.65	2850	2.9	2450	2.9
Fe II 5018	6200	49	4400	115	2700	70	2400	65
Fe II 5169	6000	38.5	4350	52	2400	45	2050	47
Fe II 5322	-	-	4700	5.0	2600	6	2400	3.4
Fe II 5429	-	-	-	-	2600	0.3	2400	0.1
Sc II 5526	-	-	-	-	2600	1.13	2200	0.40
Sc II 5657	-	-	-	-	2650	2.8	2100	1.65
Ba II 5853	-	-	-	-	2750	7.9	2500	5.5
Na I 5889	-	-	4200	0.15	2950	0.33	2500	0.3
Na I 5895	-	-	-	-	2950	0.33	2500	0.3
Ba II 6142	-	-	-	-	2600	0.27	2250	0.32
Sc II 6245	-	-	-	-	2650	0.9	2200	0.65
Sc II 6378	-	-	-	-	2600	0.07	2200	0.1
Ba II 6497	-	-	-	-	2600	0.35	2150	0.33
H α	8500	0.7	6650	0.8	4300	0.95	3850	0.85
Ca II 8498	6550	49	5300	55	3700	17	3300	21
Ca II 8542	6550	1.85	5300	1.65	3700	0.6	3300	0.47
Ca II 8662	6400	12	5300	11.5	3700	9	3200	9
C I 9088	-	-	3800	0.3	2450	0.18	-	-
Sc II 9236	-	-	-	-	2600	0.23	-	-
C I 9405	-	-	-	-	2600	0.23	-	-

Table 6: Line identifications and derived velocities, $v(\text{ph})$, (km/s) and lower level populations, $N_{\text{low}}(\text{ph})$, (cm^{-3}) for the infrared spectra

Line	22 days		44 days		69 days		85 days	
	$v(\text{ph})$	$N_{\text{low}}(\text{ph})$	$v(\text{ph})$	$N_{\text{low}}(\text{ph})$	$v(\text{ph})$	$N_{\text{low}}(\text{ph})$	$v(\text{ph})$	$N_{\text{low}}(\text{ph})$
P δ	6200	2.1	4300	0.3	3000	0.1	2350	0.3
Sr II 10327	-	-	3300	0.23	2600	0.6	2350	1.15
Fe II 10547	-	-	3300	1.65	2450	0.5	2200	0.45
C I 10695	6500	0.5	3700	0.17	2350	0.08	2200	0.1
He I 10830	-	-	6000	0.055	4250	0.21	3750	0.23
P γ	6100	1.25	4200	0.16	3200	0.27	2600	0.7
P β	6100	0.2	4200	0.15	3700	0.05	2700	0.03
P α	-	-	4700	0.04	3700	0.08	-	-
Br γ	-	-	4100	0.08	3000	0.04	-	-

Table 7: Rates for the depopulation processes of the $2s^3S$ level.

Depopulation process	Rate s^{-1}
Radiative decay	1.24×10^{-4}
Collisions to singlet states	1.8×10^{-2}
$2s^3S \rightarrow 2p^3P \rightarrow 1s^1S$	4×10^{-3}
Penning ionisation	92

Table 8: Results of the modelling and ^{56}Ni mass estimates

χ_{He}	k	v_c (km/s)	^{56}Ni mass in the power law zone ($\times 10^{-2} M_{\odot}$)	^{56}Ni mass above the helium photosphere ($\times 10^{-7} M_{\odot}$)
0	8 ± 1	1150 ± 300	2.43 ± 0.25	750 ± 26
0.1	9.5 ± 1.5	880 ± 350	2.05 ± 0.24	19 ± 1.5
0.2	9 ± 1	650 ± 200	2.1 ± 0.18	6.3 ± 0.43

Figure Captions

Figure 1: Optical spectra of SN 1995V taken with the Isaac Newton Telescope, La Palma (see Table 1 for details). The fluxes have been scaled as explained in the text. For clarity the spectra have been displaced vertically by the amounts indicated. The days shown are with respect to the estimated date of shock breakout, 25 July 1995.

Figure 2: Comparison of the B light curve of the type IIp SN 1983 K (Phillips *et al.* 1990) with the uncorrected B magnitudes for SN 1995V derived from the spectra. To aid the comparison, the SN 1995V points have been vertically displaced by -3.5 magnitudes. The upper limit of Evans (1995) on 25 July 1995 is also indicated. This, together with the four B magnitudes, enables us to fix the time of shock break-out, t_0 , to a precision of ± 2 days.

Figure 3: Infrared spectra of SN 1995V taken with the Anglo-Australian Telescope (days 22 and 85) and the United Kingdom Infrared Telescope (days 42, 44 and 69) (see Table 3 for details). The fluxes have been scaled as explained in the text. For clarity the spectra have been displaced vertically by the amounts indicated. The days shown are with respect to the estimated date of shock breakout, 25 July 1995.

Figure 4: Observed optical spectra of SN 1995V compared with the spectral model. Details of the model parameters, line velocities and populations of the transition lower levels are presented in Tables 4 and 5. Absorption minima of identified lines are indicated.

Figure 5: Observed infrared spectra of SN 1995V compared with the spectral model. Details of the model parameters, line velocities and populations of the transition lower levels are presented in Tables 4 and 6. Absorption minima of identified lines are indicated.

Figure 6: Comparison of two model fits for 69 and 85 days. The dashed line represents the model fit when He I 10830 Å is *not* included. The model fit which includes He I 10830 Å (solid strong line) is clearly superior.

Figure 7: Synthetic spectra produced using the ^{56}Ni density profile of the explosion model s15s7b2f compared with observations. The quantity χ_{He} indicates the fraction of the helium mass that was in the form of clumps for each model.

Figure 8: The ^{56}Ni density profile used to represent the dredge-up of the radioactive material

Figure 9: ^{56}Ni density profiles that produce the best fit synthetic spectra. (The helium photosphere lies at ~ 4250 km/s for day 69)

Figure 10: Synthetic spectra produced using the ^{56}Ni profile of figure 8 with parameters $k = 9.0$, $v_c = 800$ km/s and assuming that 10% of the helium mass was in the form of clumps.

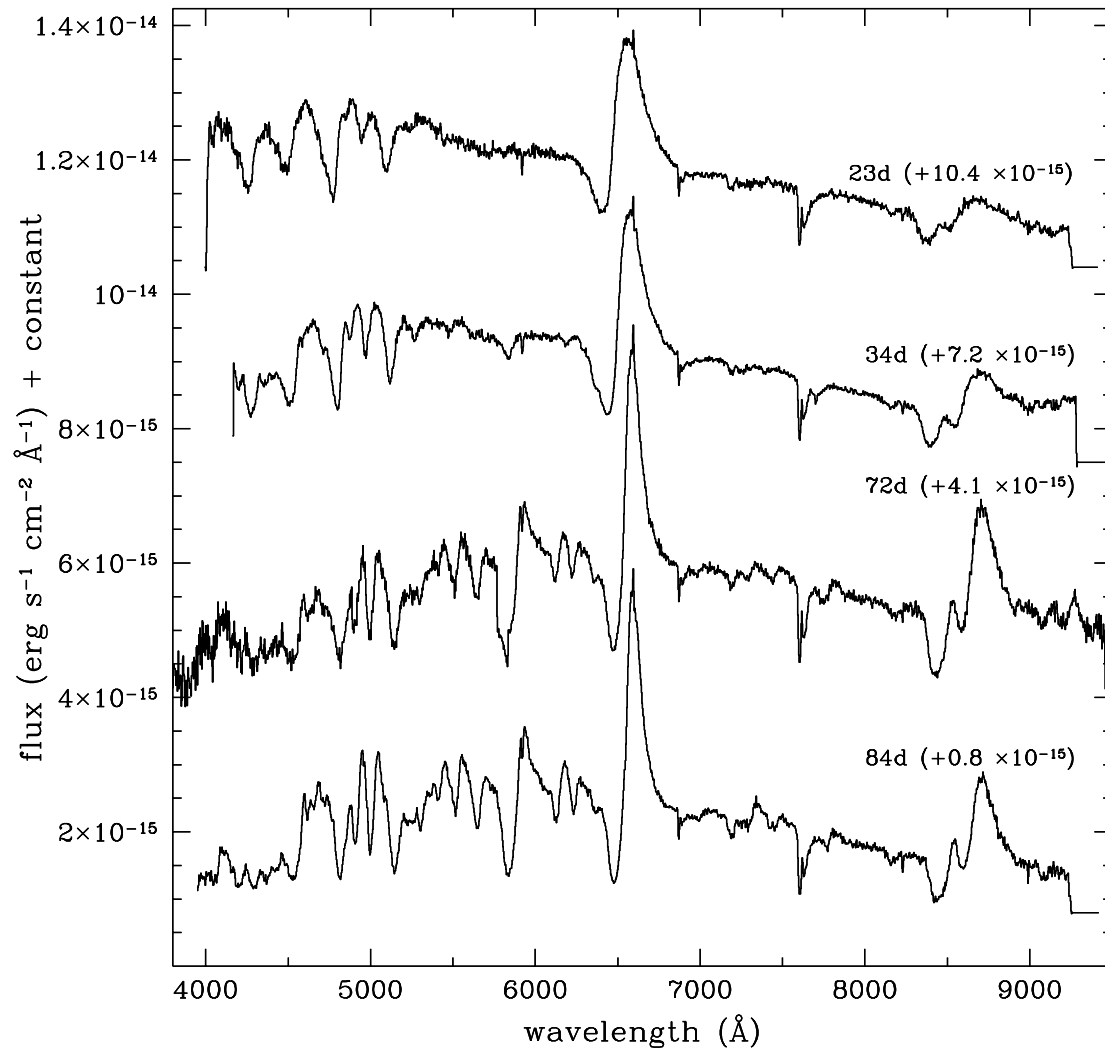


Figure 1:

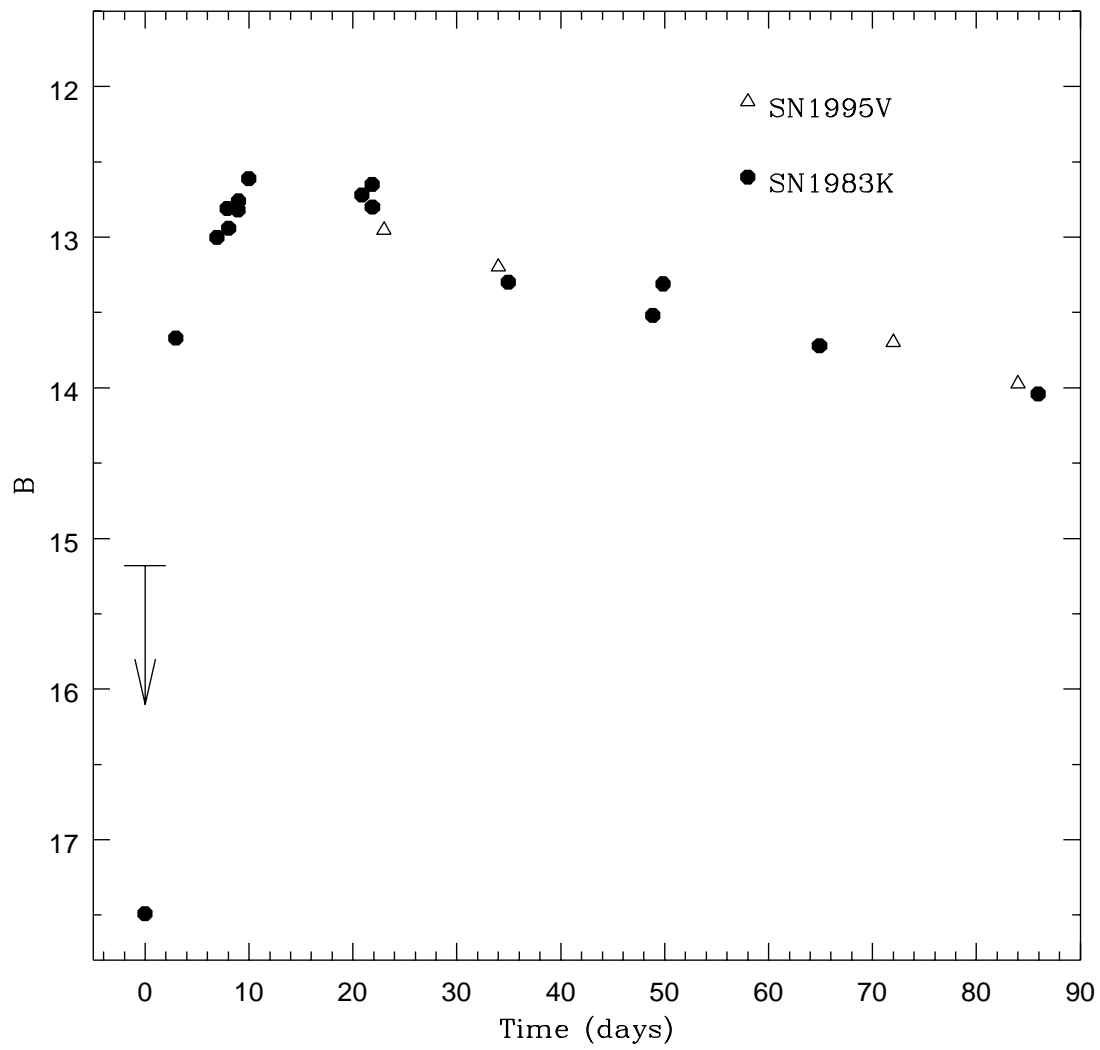


Figure 2:

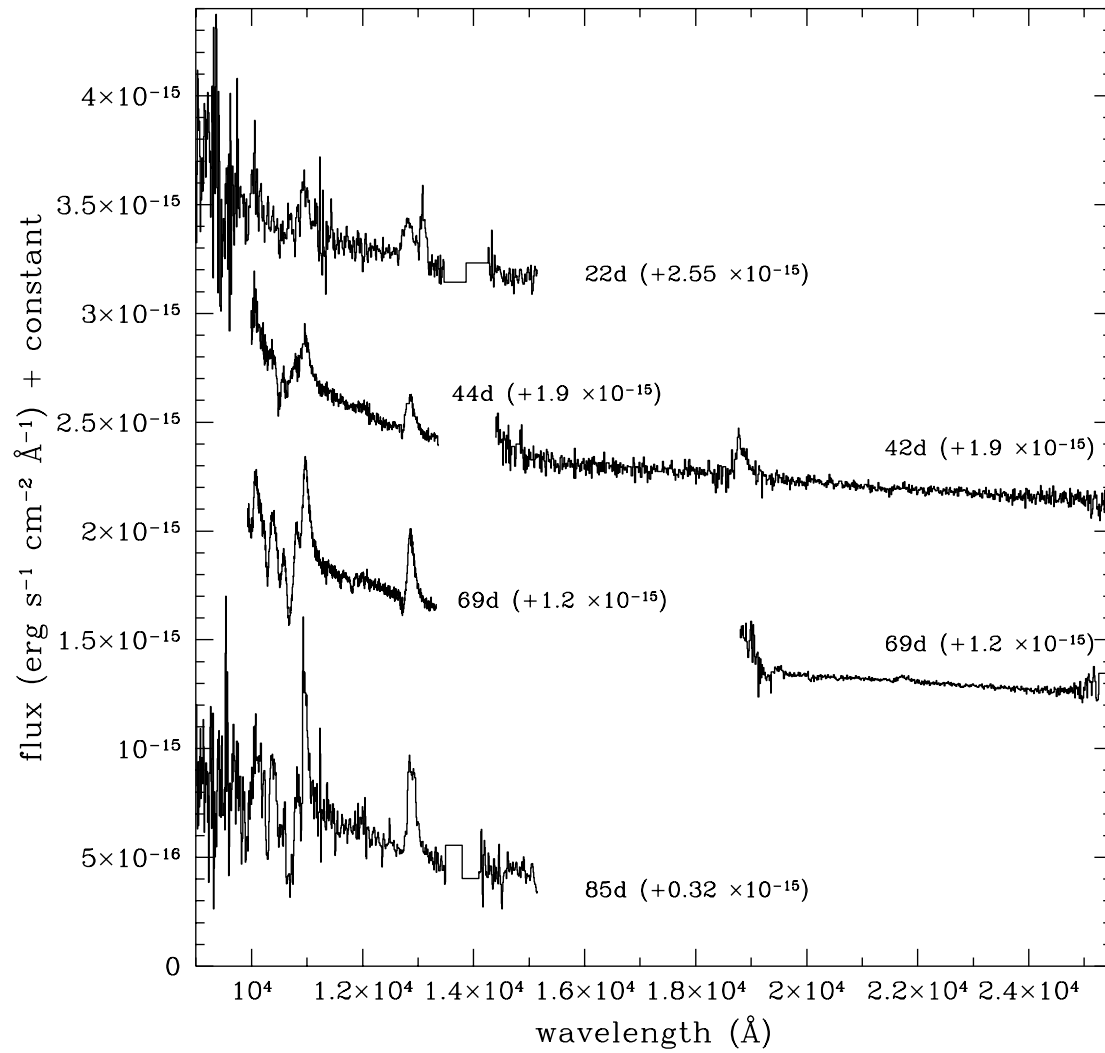


Figure 3:

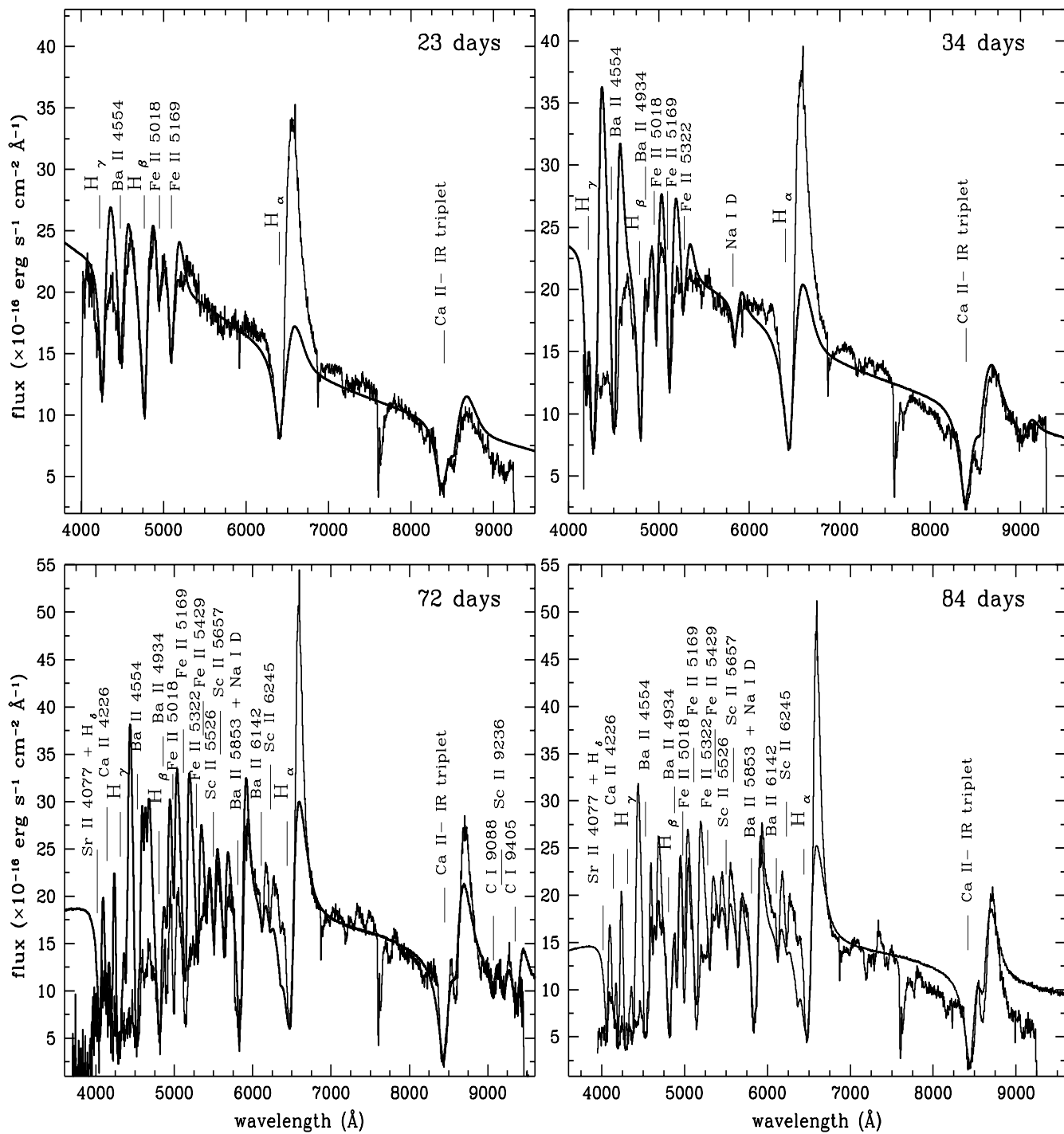


Figure 4:

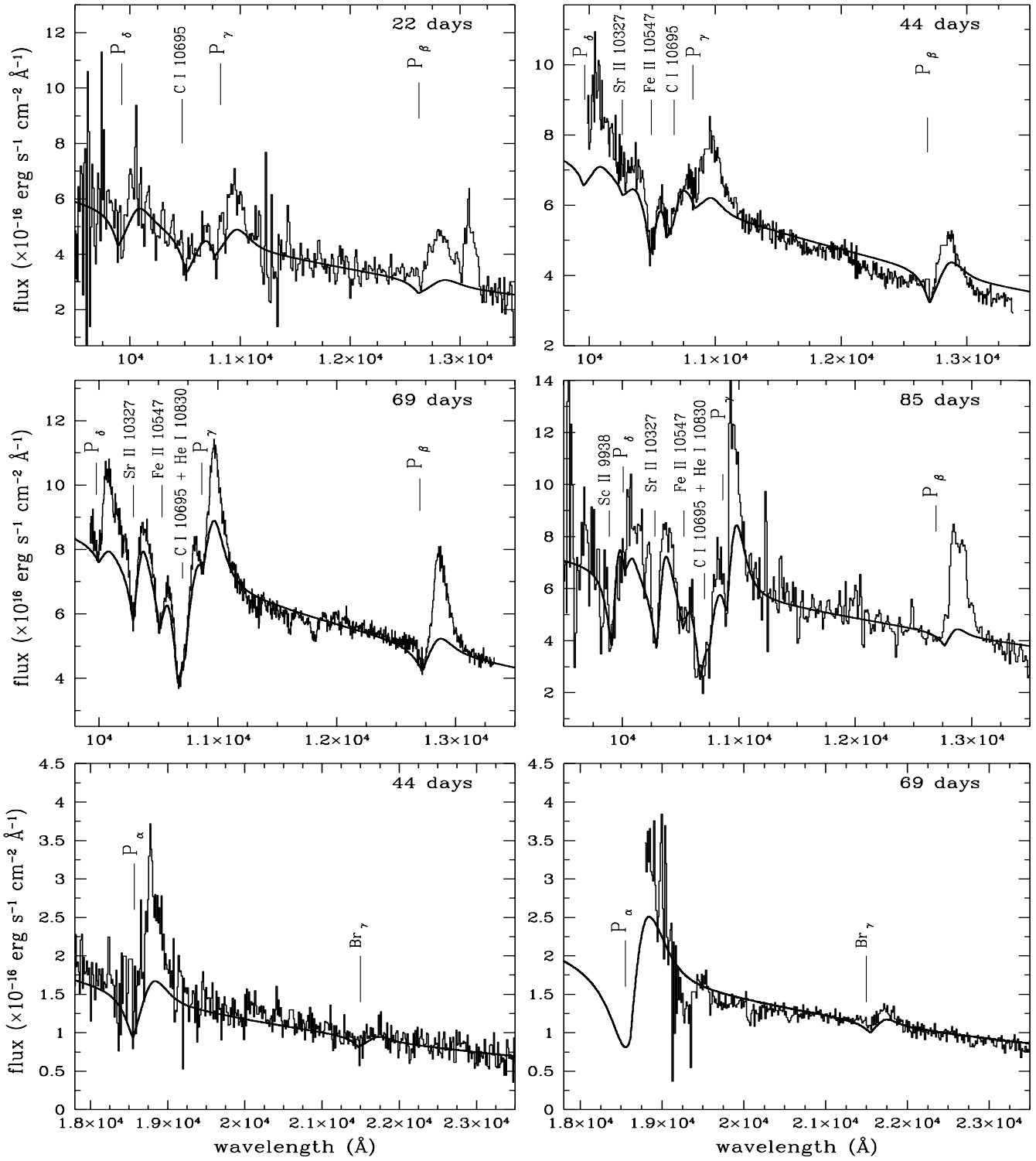


Figure 5:

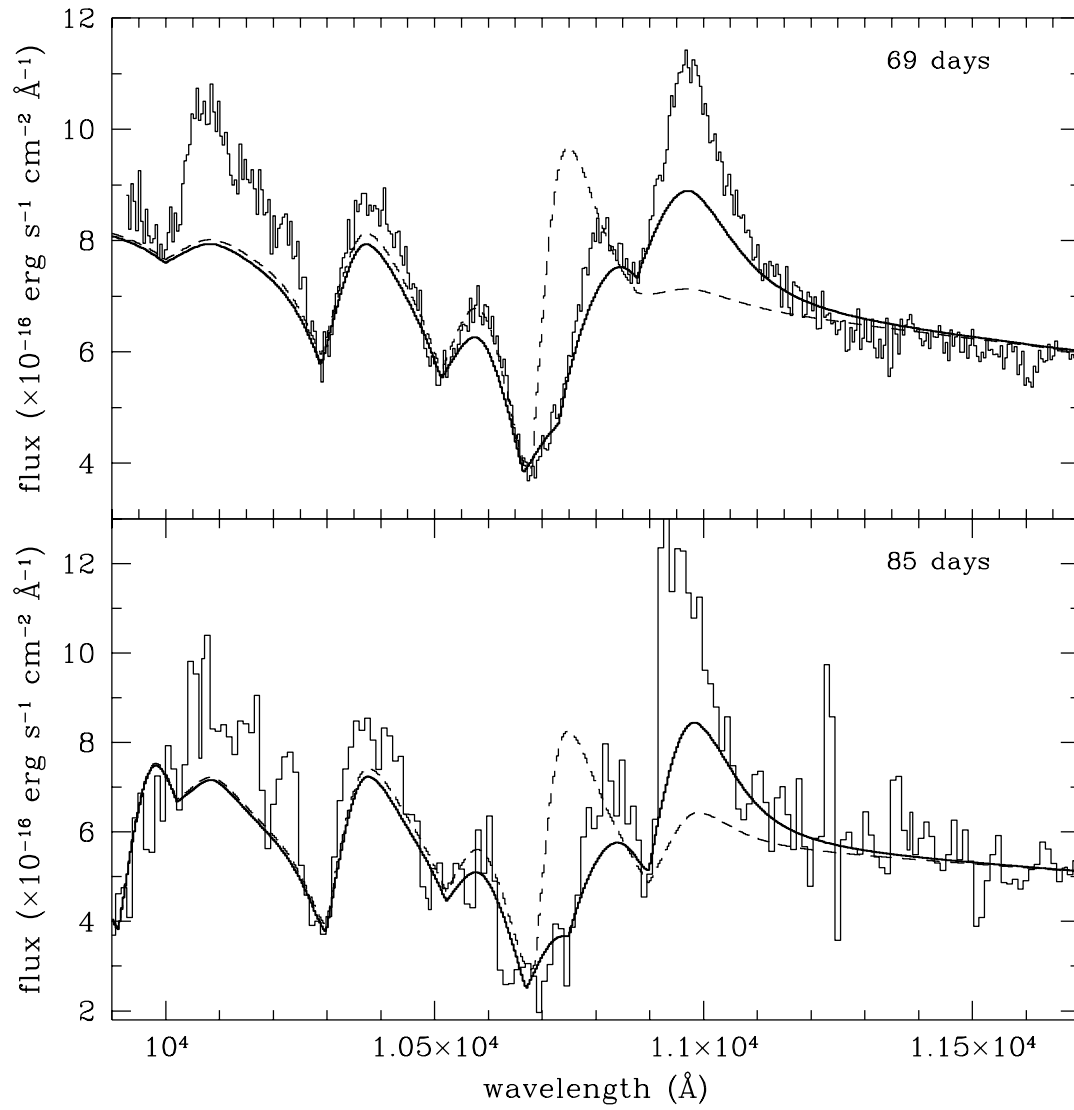


Figure 6:

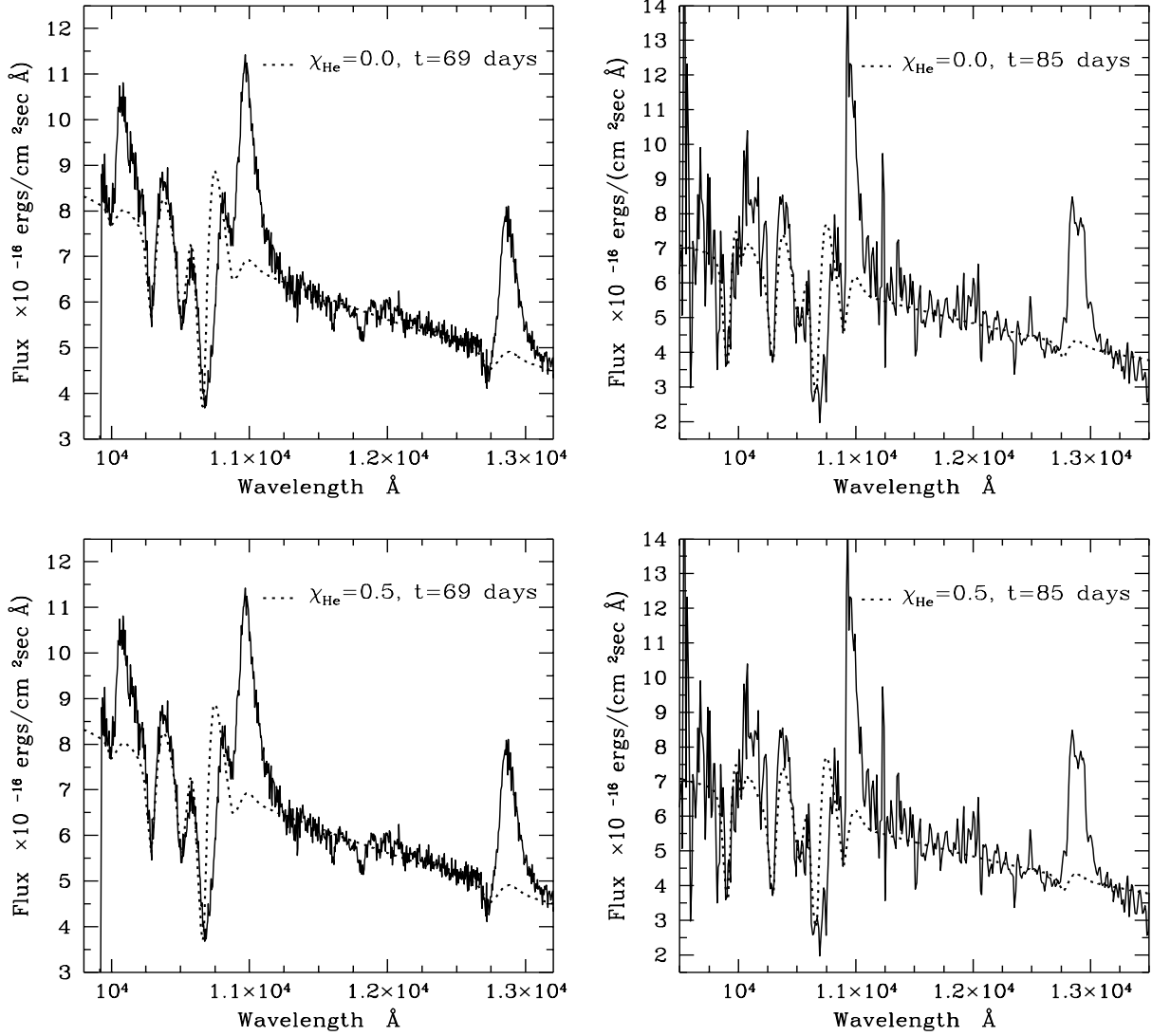


Figure 7:

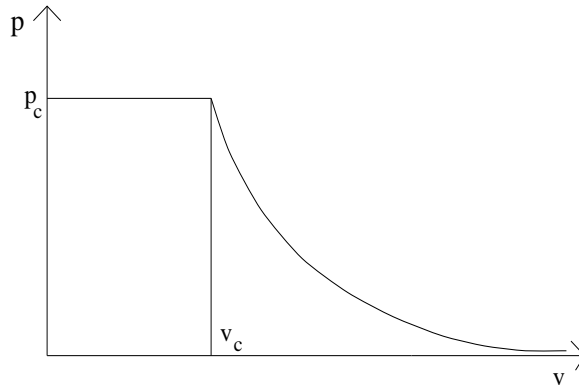


Figure 8:

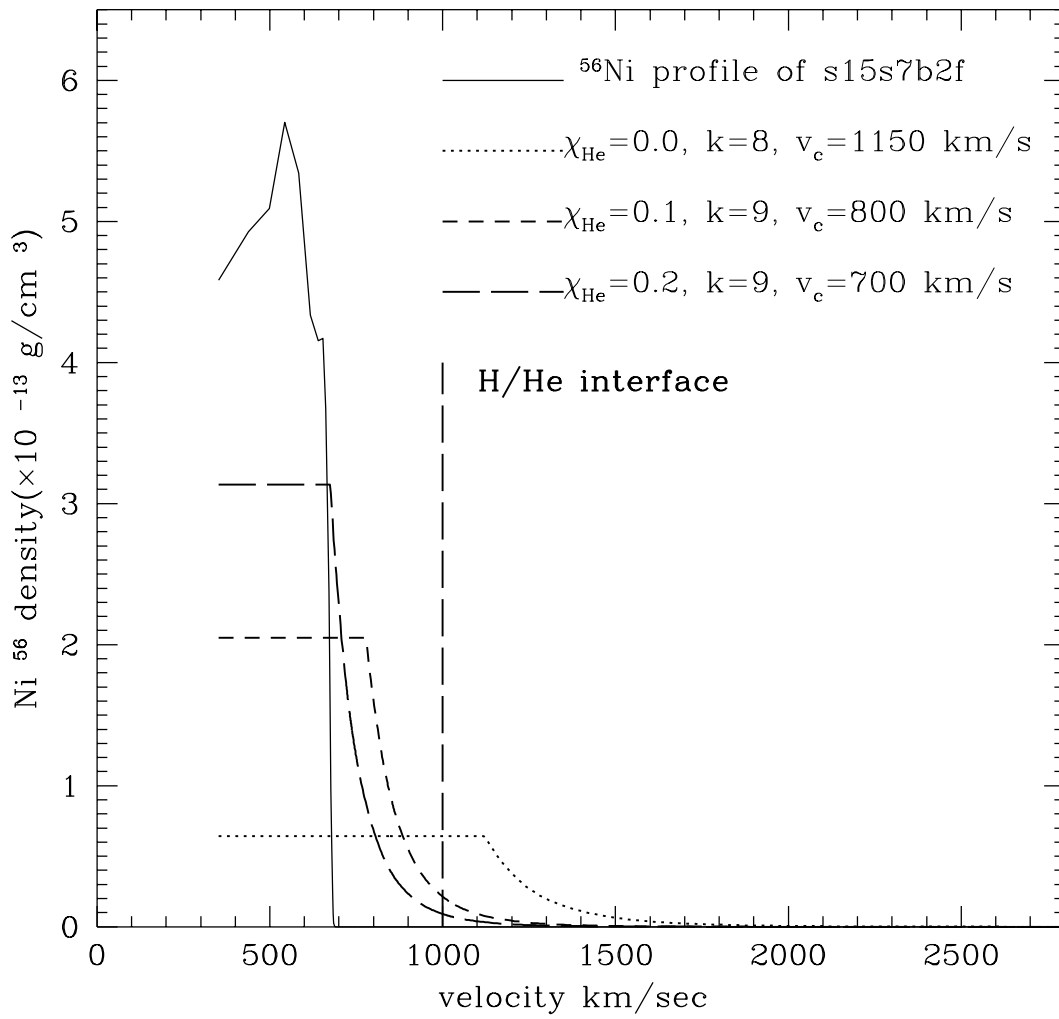


Figure 9:

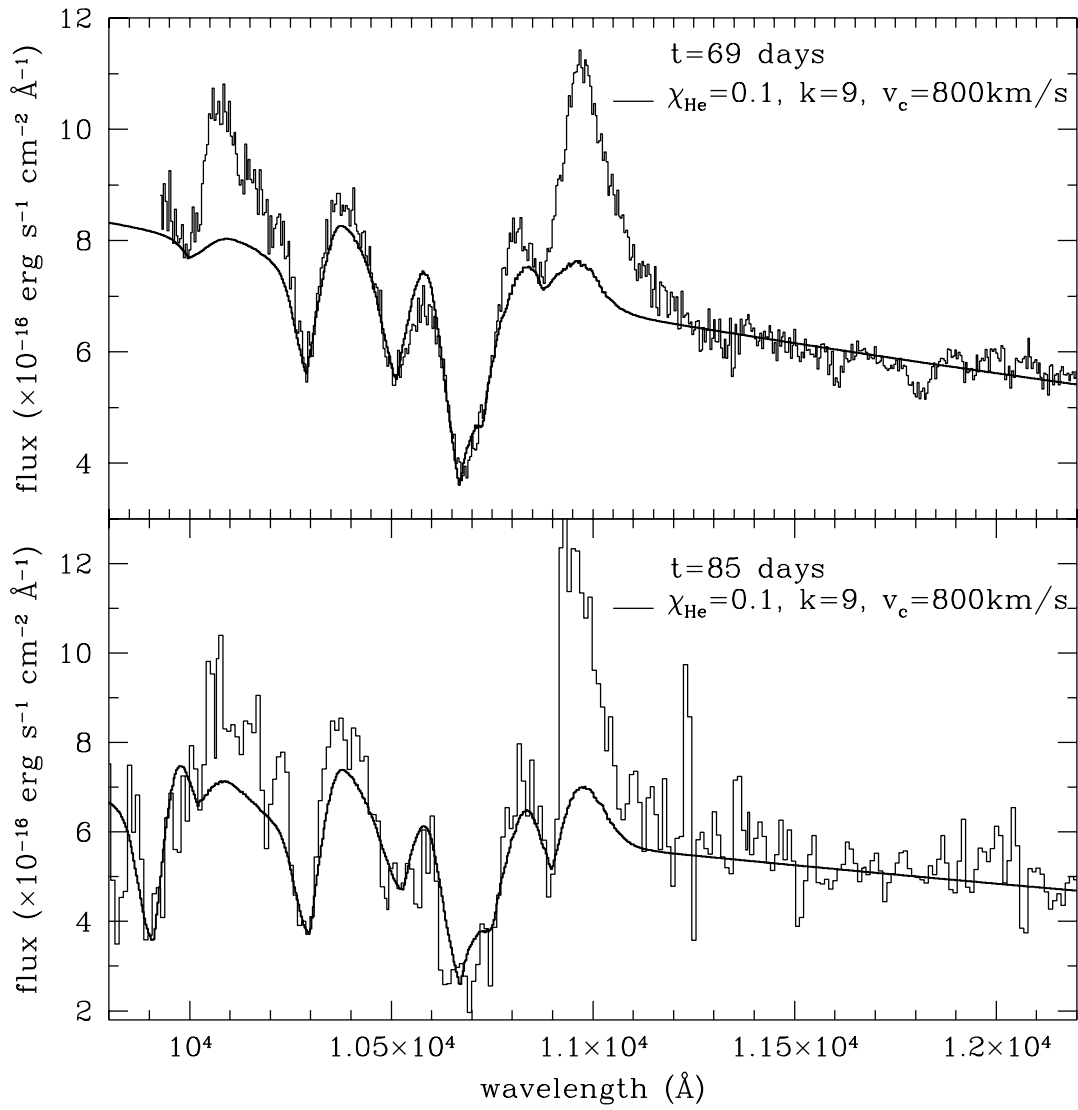


Figure 10: